Current Biology *16*, 1962–1967, October 10, 2006 DOI 10.1016/j.cub.2006.08.027

Report

Mitosis-Specific Mechanosensing and Contractile-Protein Redistribution Control Cell Shape

Janet C. Effler,[1,2] Yee-Seir Kee,[1] Jason M. Berk,[1] Minhchau N. Tran,[1] Pablo A. Iglesias,[2] and Douglas N. Robinson[1,*]
[1] Department of Cell Biology
Johns Hopkins University School of Medicine
[2] Department of Electrical and Computer Engineering
Johns Hopkins University Whiting School of Engineering
725 N. Wolfe Street
Baltimore, Maryland 21205

Summary

Because cell-division failure is deleterious, promoting tumorigenesis in mammals [1], cells utilize numerous mechanisms to control their cell-cycle progression [2–4]. Though cell division is considered a well-ordered sequence of biochemical events [5], cytokinesis, an inherently mechanical process, must also be mechanically controlled to ensure that two equivalent daughter cells are produced with high fidelity. Given that cells respond to their mechanical environment [6, 7], we hypothesized that cells utilize mechanosensing and mechanical feedback to sense and correct shape asymmetries during cytokinesis. Because the mitotic spindle and myosin II are vital to cell division [8, 9], we explored their roles in responding to shape perturbations during cell division. We demonstrate that the contractile proteins myosin II and cortexillin I redistribute in response to intrinsic and externally induced shape asymmetries. In early cytokinesis, mechanical load overrides spindle cues and slows cytokinesis progression while contractile proteins accumulate and correct shape asymmetries. In late cytokinesis, mechanical perturbation also directs contractile proteins but without apparently disrupting cytokinesis. Significantly, this response only occurs during anaphase through cytokinesis, does not require microtubules, and is independent of spindle orientation, but is dependent on myosin II. Our data provide evidence for a mechanosensory system that directs contractile proteins to regulate cell shape during mitosis.

Results and Discussion

To test whether cells monitor their shape during cell division, we examined whether cytokinetic *Dictyostelium discoideum* cells show asymmetries in myosin-II distribution, which would be suggestive of an active system for correcting shape asymmetries. We collected and analyzed 40 time-lapse movies of dividing *myoII*::GFP-myosin-II; RFP-α-tubulin cells. Of these, 57% showed symmetric myosin-II distribution and centralized spindle placement during cytokinesis and an enrichment of myosin II in the cleavage furrow as cytokinesis progressed (Figure 1A; Table S1 and Movie S1 in the Supplemental Data available online). However, the remaining 43% exhibited an asymmetrically positioned mitotic spindle early (anaphase to onset of furrowing) in cytokinesis, with GFP-myosin-II distribution concentrated in the cortex furthest from the spindle. These asymmetrical cells had an axial ratio of 1.5 ± 0.08 (mean ± standard error of the mean [SEM]), which is significantly greater than the axial ratio of 1.2 ± 0.03 for the symmetrically shaped cells (Student's t test, $p = 0.001$; Supplemental Experimental Procedures). As the cells progressed through anaphase, the spindle was repositioned to the center, and myosin II accumulated at the equator, allowing the cells to proceed symmetrically through cytokinesis (Figure 1B; Table S1; Movie S2). These observations suggest that cells redistribute myosin II to correct shape and/or spindle asymmetries, preventing the cell from producing asymmetric daughter cells.

Because cell-shape deformation and force are inextricably linked, we tested the possibility that shape asymmetry reflects asymmetric forces acting on the cell cortex. To determine rigorously whether myosin-II asymmetry is a response to shape disturbances, we developed a micropipette aspiration system to apply mechanical loads to dividing cells (Supplemental Experimental Procedures). To ensure that physiologically relevant loads were applied, the minimum pressure required to form a small hemispherical bulge in the pipette was used. Commensurate with the cortical tension of the cell, this load should generate significant cellular deformation (strain) without overwhelming the ability of the cell to respond mechanically. Aspiration pressures applied to *myoII*::GFP-myosin-II; RFP-α-tubulin ranged from 0.16–0.60 nN/μm^2. On the basis of the pipette radius and pressure, the applied force ranged from 8–15 nN, similar to the 4–7 nN of force estimated previously to drive the shape changes of cytokinesis [10, 11].

Using this system, we demonstrate that cells recruit contractile proteins in response to shape deformation to regulate the progression of shape changes during cytokinesis. When aspiration pressure was applied to cells in early (anaphase to the onset of furrowing) or late (onset of furrowing to completion) cytokinesis, *myoII*::GFP-myosin-II; RFP-α-tubulin cells responded by sending GFP-myosin II to the cortex in the pipette (Figure 2A; Table S1; Movie S3). To analyze the responses quantitatively, we measured GFP-myosin-II cortical intensities inside and outside the pipette (Supplemental Experimental Procedures; Figures 2D–2F). Cells aspirated early in cytokinesis generated large-scale myosin-II responses, resulting in substantial recruitment of GFP-myosin II to the pipette, enabling the cell to reject the shape disturbance even though the applied mechanical load was kept constant (Figures 2A and 2D). After escaping the pipette, myosin II redistributed to the furrow and the cell divided symmetrically. A small-scale

*Correspondence: dnr@jhmi.edu

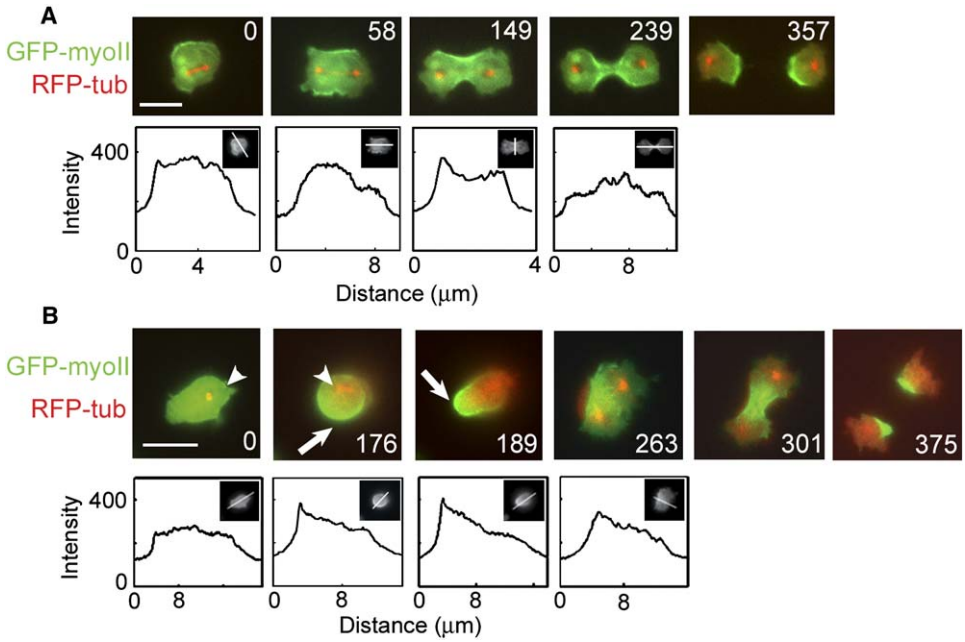

Figure 1. Progression of a Mitotic Cell through the Stereotypical Shape Changes of Cytokinesis without Mechanical Load

(A) Symmetrical GFP-myosin II is observed in 57% of unloaded dividing cells. The cell rounded up, and the mitotic spindle was centrally positioned (0 s). GFP-myosin II enriched in the cleavage furrow and the mitotic spindle elongated, positioning each daughter nucleus at opposite poles (58 s). The cleavage furrow constricted (149 s) until a bridge was formed (239 s), which finally severed (357 s). Line scans show the magnitude of GFP-myosin II; insets show the line position. This sequence corresponds to Movie S1.

(B) Asymmetric GFP-myosin-II distribution in early cytokinesis is found in 43% of dividers. Initially, the cell is elongated with the mitotic spindle asymmetrically positioned within the cell (0 s, arrowheads). GFP-myosin II localized to the polar cortex (arrows; 176 s) furthest from the spindle. As the spindle elongated (189 s and 263 s), myosin II reoriented to the cleavage furrow, and the cell progressed through symmetric shape changes of cytokinesis (375 s). Line scans revealed the magnitude of the GFP-myosin-II response; insets show the line position. The line scan of the 263 s frame shows the asymmetry of myosin II in the cleavage-furrow cortex (compares to Figure 1A 149 s). Scale bars represent 10 μm. This sequence corresponds to Movie S2.

myosin-II response was observed in cells that were loaded late in cytokinesis (Figures 2B and 2E). In these late-stage cytokinetic cells, myosin II accumulated in the polar cortex without apparently disrupting the myosin-II accumulation at the contractile ring. Under continuous load, these cells divided symmetrically. Significantly, cells perturbed by the pipette took longer (630 ± 63 s, n = 27) to complete cytokinesis than unloaded cells (460 ± 24 s, n = 23; Student's t test, p = 0.017). To determine the completion times, we used the initiation of spindle elongation as the reference time (0 s), which meant only movies of cells starting prior to anaphase onset could be included in the completion-time analysis. Overall, the majority of aspirated mitotic cells (73%) responded by localizing myosin II to the site of aspiration, demonstrating their ability to respond to mechanical disturbances during cytokinesis (Table S1).

To test whether the redistribution of myosin II in response to mechanical load is mitosis specific or is a general mechanosensory response, we examined interphase cells. Interphase cells expressing GFP-myosin II were aspirated with pressures ranging from 0.2–0.6 nN/μm^2 for over 25 min, ~25-fold longer than needed for a response during mitosis (Figure 2C). Of 17 interphase cells, none recruited myosin II to the pipette (Figures 2C and 2F; Table S1). Because the half-life for myosin II at the cortex is similar in interphase and mitotic cells [12], the response likely depends on a mitosis-specific mechanosensor that is independent of myosin-II thick-filament assembly and localization dynamics.

Because aspiration applies force to the cell and myosin II is a force-generating mechanoenzyme, we tested whether myosin II is required for resisting the applied force to ensure symmetrical cytokinesis. Without mechanical load, approximately half (compared to only 8% of wild-type unloaded divisions and 5% of wild-type loaded divisions) of the successful myosin-II mutant cell divisions produced unequally sized daughter cells, and the overall failure rate of cell division was not appreciably higher for myosin-II mutant cells than for wild-type cells (Table S2). When aspirated, the myosin-II mutant cells showed a 3-fold increase in failure rate and lost their ability to control their shape changes, leading to grossly asymmetric divisions (Figures 3A and 3B; Table S2; Movie S4). Furthermore, the myosin-II mutant cells could only withstand about half of the aspiration pressure as wild-type cells without being fully aspirated into the pipette. Thus, myosin II is essential for resisting mechanical disturbances and for ensuring symmetrical cell division.

We also examined whether other actin-associated cytoskeletal proteins respond to mechanical load. Cells expressing GFP-cortexillin I, an actin crosslinker that localizes to the cleavage-furrow cortex during cytokinesis, were aspirated with pressures ranging from

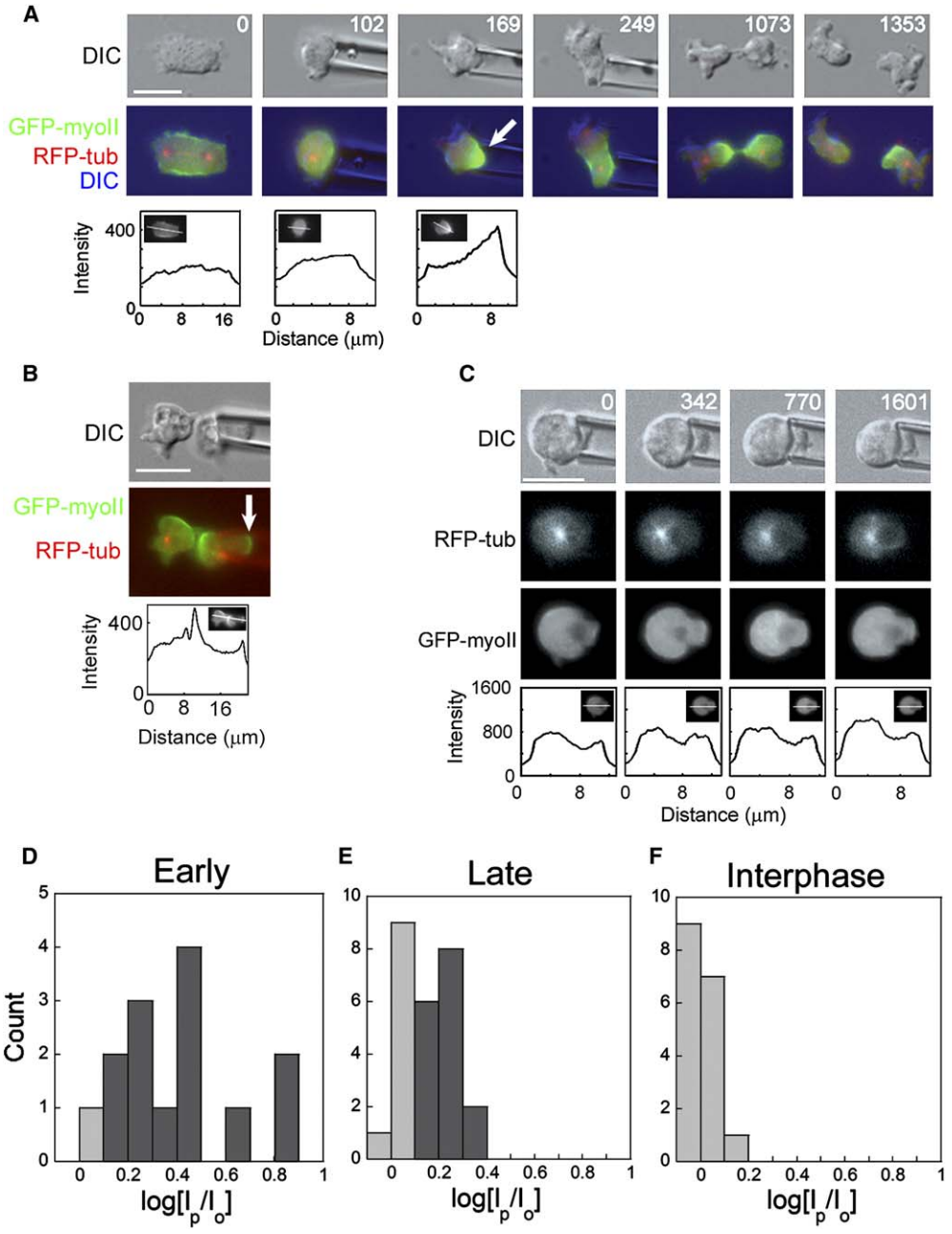

Figure 2. GFP-myosin II Localized in Response to Mechanical Load in Cells Undergoing Cytokinesis

(A) A mitotic cell in early cytokinesis (0 s) was captured with the micropipette aspirator (102 s) by using a pressure of 0.34 nN/μm^2. Although a contractile ring had been initially formed (0s), the cell recruited GFP-myosin II to the pipette (169 s). Under constant pressure, the cell escaped the pipette (249 s). The cell reoriented myosin II to the equator, re-established the correct spindle position, and underwent symmetric cytokinesis (1073 s, 1353 s). Line scans show the magnitude of the GFP-myosin-II response; insets show the line position. The 169 s panel can be compared to the 189 s panel in Figure 1B, which also shows asymmetric myosin II. This image sequence corresponds to Movie S3.

(B) A cell aspirated late in cytokinesis accumulated GFP-myosin II to both the pipette and the furrow. Even under continuous load, the cell divided. Line scan shows the magnitude of the GFP-myosin-II response; insets show the line position. This cell can be contrasted to the 239 s panel in Figure 1A, where there is no polar enrichment of myosin II.

(C) An interphase cell was aspirated with a pressure of 0.3 nN/μm^2 for 26 min. GFP-myosin II was not recruited to the site of the pipette, indicating that GFP-myosin-II recruitment is mitosis specific. Line scans show the magnitude of the GFP-myosin-II response; insets show the line position. Scale bars in (A)–(C) represent 10 μm.

(D)–(F) Frequency histograms of the distribution of magnitudes of early (D) and late (E) cytokinesis and interphase (F) responses. Responders (Supplemental Experimental Procedures) are shaded dark gray, and nonresponders are shaded light gray. Both early and late distributions were significantly greater than the interphase responses (Student's t test: $p < 0.0001$). As a note, we have yet to detect a clear correlation between the magnitudes of the applied loads and responses.

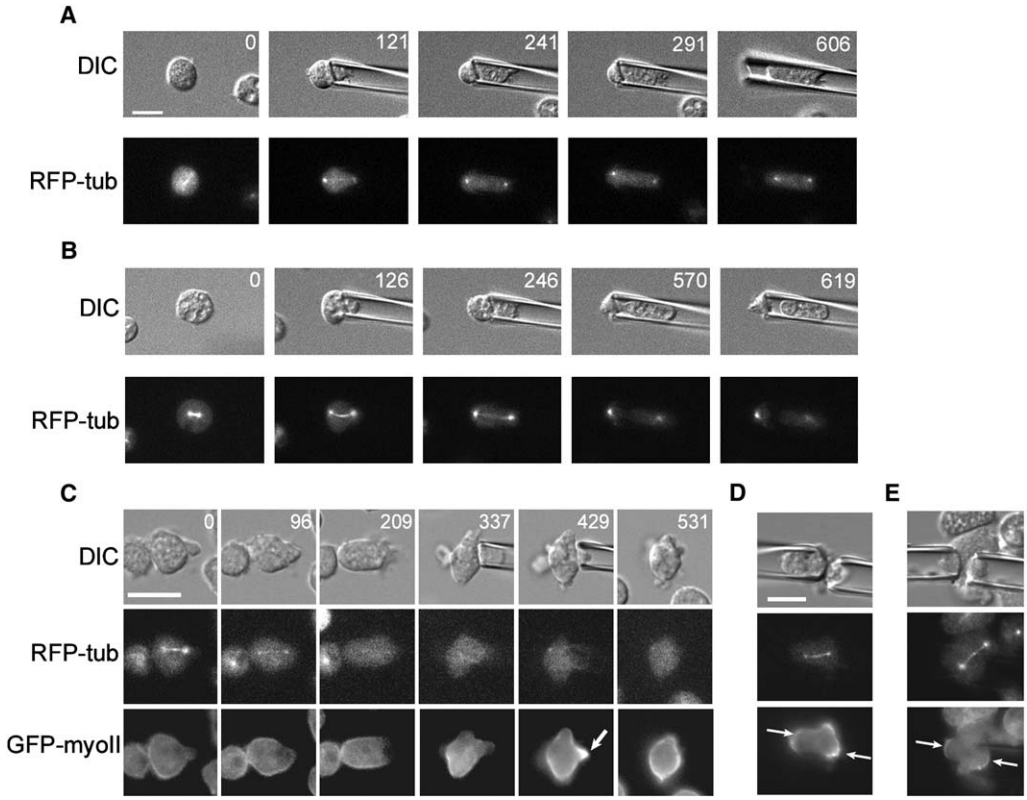

Figure 3. Contractile Proteins Control Cell Chape during Cytokinesis and Redistribute in Response to Load Independent of Microtubules

(A) The *myoII* null cell fails to divide under pressure (0.16 nN/μm^2). Movie S4 shows a different myosin-II mutant cell failing cytokinesis under load.

(B) The *myoII* null cell divides under pressure (ranging from 0.1–0.2 nN/μm^2), producing two grossly asymmetric daughter cells. Scale bar represents 10 μm and applies to all panels in (A) and (B).

(C) Microtubules were inhibited with nocodazole (added at 21 s). Aspiration pressure (0.35 nN/μm^2) was applied after the microtubules disappeared (337 s). GFP-myosin II localized to the pipette without microtubules (arrow, 429 s). This image sequence corresponds to Movie S6.

(D) With the pipettes aligned parallel to the spindle axis, crescents (arrows) of myosin II assembled at each polar cortex. The aspiration pressure was 0.45 nN/μm^2.

(E) Crescents (arrows) of myosin II assembled on opposing sides of the spindle with two pipettes oriented perpendicularly to the mitotic spindle but placed near one centrosome. The aspiration pressure was 0.35 nN/μm^2.

0.15–0.30 nN/μm^2. Cortexillin I was recruited to the site of the applied load in 67% of dividing cells (Figure S1; Table S1; Movie S5). However, similar to myosin II, cortexillin I failed to redistribute in response to mechanical disturbance during interphase (Table S1). In contrast, dynacortin, which enriches in the polar cortex during cytokinesis, did not relocalize to the pipette during mitosis (Figure S2). Thus, the mechanosensory system is a contractile-protein response, rather than a myosin-II-specific or a general cytoskeleton response.

The mitotic spindle delivers positive and negative signals to the overlying cortex, which triggers contractile-ring assembly [8]. In our experiments, all of the unloaded cells and 64% of the loaded cells that had asymmetric GFP-myosin-II distribution during early cytokinesis also had an asymmetrically positioned mitotic spindle. Although cells were aspirated during all stages of mitosis, cells exclusively responded to mechanical load by redistributing contractile proteins during anaphase through the end of cytokinesis. These observations raise the question of whether the GFP-myosin-II recruitment is a response to an asymmetrically positioned anaphase spindle, applied load, or both. To separate the roles of force from spindle position, we used nocodazole to depolymerize the microtubules during anaphase (Supplemental Experimental Procedures). Myosin II redistributed in response to aspiration in the absence of microtubules, and, further, the myosin-II response dissipated when the pressure was released, indicating that force was sufficient to direct myosin-II recruitment (Figure 3C; Table S1; Movie S6). Using two pipettes to apply load to different regions of the cortex simultaneously, we also verified that spindle orientation did not influence the ability to respond to mechanical load. Crescents of myosin II could be recruited to the cortex under each pipette with the spindle in any orientation with respect to the pipettes (Figures 3D and 3E).

These observations, coupled with the response in late cytokinesis (Figure 2B), demonstrate that mechanical force deforms the cortex, leading to the redistribution of contractile proteins, and that applied force can override normal spindle signals (Figure 1A versus Figure 3D). Thus, although the mitotic-spindle position correlates with the asymmetric distribution of contractile proteins, its role is not essential for mechanosensing. Therefore, the asymmetry in spindle position may be reflective of

asymmetric cell shape and/or mechanical strain in the cortical network.

Historically, micromechanical studies have contributed significantly to our understanding of the changes in mechanical behavior that correlate with cytokinetic furrowing [9, 13–17]. However, the molecular bases for these changes, how they relate to cleavage-furrow ingression, and how they regulate the evolution of cell shape are not understood [9, 18]. Our study raises the possibility that some of the mechanical changes uncovered by traditional micromechanical techniques may have been influenced by mechanosensory responses of dividing cells. Previous studies also demonstrated that contractile proteins can be directed around the cell by moving the spindle [19, 20]; however, our observations indicate that applied force can override normal spindle signals, allowing myosin II to accumulate wherever cell-shape deformation is induced (Figure 4).

Numerous biological systems achieve robustness by utilizing feedback loops [21, 22]. We propose that this mechanosensory system of redistributing proteins in response to shape perturbations is part of a feedback mechanism that monitors cell shape. In this feedback system, mechanical strain in the network triggers activation of a mechanosensor, leading to recruitment of myosin II and cortexillin I to the shape disturbance. These proteins then increase the local viscoelastic resistance of the cortex [9, 23, 24], slowing further shape deformation. During early cytokinesis, furrowing is delayed until myosin II, which promotes dynamic cortical rearrangements through its mechanochemistry [24], contracts the cortex away from the pipette. During late cytokinesis, myosin II recruited to the pipette at the polar cortex resists the local deformation, whereas equatorial myosin-II contractility along with other myosin-II-independent processes (Laplace pressures and membrane trafficking [11, 25]) continue furrow thinning. Further, the ability to correct mechanical perturbation is dependent on myosin II, and cells deficient in either myosin II or cortexillin I have increased frequencies of asymmetrical cell divisions, indicating an inability to correct shape asymmetries (Table S2, [23, 26]). Importantly, loaded wild-type cells achieve levels of cytokinesis completion similar to those of unloaded cells (Table S1), demonstrating the robustness of this system.

Significantly, this system is mitosis specific, suggesting a novel pathway for mechanosensation. Cells must sense mechanical strain in the cortex, perhaps by opening ion channels or by stretching cortical cytoskeletal proteins to create new binding sites [6, 7], triggering contractile-protein recruitment. Previous studies on interphase *Dictyostelium* and mammalian cells have shown that extreme cell deformation leads to cortex-membrane rupture and myosin-II recruitment to the rupture site [27, 28]. However, our response is specific to anaphase through cytokinesis and does not appear to involve cortex-membrane rupture. Microtubule depolymerization also promotes oscillatory myosin-II-dependent contractions of interphase cells [29, 30]. In contrast, our response occurs in the presence of microtubules with and without external mechanical perturbation and is not oscillatory. The mitosis specificity might arise because the contractile system is more mobile as the cell prepares for cytokinesis. During interphase, cells may mask the mitotic system and achieve shape control by other mechanisms such as strain-hardening the cytoskeleton through the action of other actin cross-linkers and cytoskeletal structures [6]. Overall, this study establishes a framework for a systems-level analysis of the biochemical and mechanical regulation of cell shape during cytokinesis.

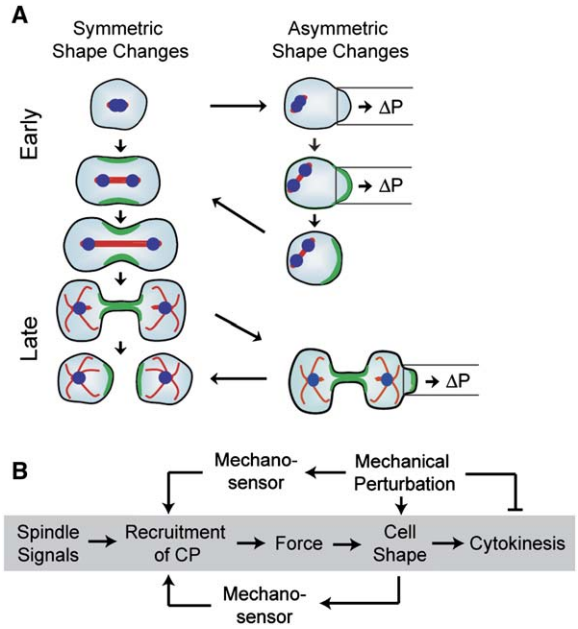

Figure 4. Mechanical Force Triggers the Redistribution of Contractile Proteins

(A) Symmetrical versus asymmetrical shape changes of cytokinesis. The left column shows the symmetrical shape changes of cytokinesis. The right column depicts the asymmetrical shape changes that either occur naturally or are induced by aspirating the cell. Cells aspirated early during anaphase recruit contractile proteins to the site of aspiration in conjunction with spindle elongation. After escaping the pipette, the cell repositions the spindle centrally and reorients myosin II and cortexillin I to the cleavage furrow, progressing through symmetrical cytokinesis. Cells aspirated late in cytokinesis recruited myosin II both to the furrow and aspirated polar region. Under continuous load, these cells typically complete symmetric division.

(B) The diagram outlines a proposed mechanical feedback system. In the unloaded (traditional) pathway (shaded gray), spindle signals initiate the process of cytokinesis, recruiting contractile proteins (CP) to the cleavage furrow. These contractile proteins generate force, driving cell-shape changes that produce cytokinesis. By applying a mechanical perturbation (load), a mechanical feedback is suggested. Mechanosensors may measure mechanical perturbations directly by measuring molecular scale strain (upper pathway) or indirectly by monitoring cell shape (lower pathway). The essential differences between these two types of mechanosensors are the length scales and magnitudes of the strains that they detect. The feedback system then leads to the recruitment of contractile proteins, which correct for shape asymmetries.

Supplemental Data

Supplemental Data include Experimental Procedures, two figures, and two tables and are available with this article online at: http://www.current-biology.com/cgi/content/full/16/19/1962/DC1/.

Acknowledgments

We thank the members of the Robinson Lab for many helpful discussions and Sue Craig (Johns Hopkins) and Yixian Zheng (Carnegie

Institution) for reading the manuscript. This work was supported by a Burroughs-Wellcome Career Development Award (D.N.R.), a Beckman Young Investigator Award (D.N.R.), the National Institutes of Health (R01#GM066817 to D.N.R., GM071920 to P.A.I.), and the National Science Foundation (DMS0083500 to P.A.I.).

Received: June 22, 2006
Revised: August 8, 2006
Accepted: August 9, 2006
Published: October 9, 2006

References

1. Fujiwara, T., Bandi, M., Nitta, M., Ivanova, E.V., Bronson, R.T., and Pellman, D. (2005). Cytokinesis failure generating tetraploids promotes tumorigenesis in p53-null cells. Nature *437*, 1043–1047.
2. Stukenberg, P.T. (2004). Triggering p53 after cytokinesis failure. J. Cell Biol. *165*, 607–608.
3. O'Connell, C.B., and Wang, Y. (2000). Mammalian spindle orientation and position respond to changes in cell shape in a dynein-dependent fashion. Mol. Biol. Cell *11*, 1765–1774.
4. Norden, C., Mendoza, M., Dobbelaere, J., Kotwaliwale, C.V., Biggins, S., and Barral, Y. (2006). The nocut pathway links completion of cytokinesis to spindle midzone function to prevent chromosome breakage. Cell *125*, 85–98.
5. Wu, J.-Q., Kuhn, J.R., Kovar, D.R., and Pollard, T.D. (2003). Spatial and temporal pathway for assembly and constriction of the contractile ring in fission yeast cytokinesis. Dev. Cell *5*, 723–734.
6. Janmey, P.A., and Weitz, D.A. (2004). Dealing with mechanics: Mechanisms of force transduction in cells. Trends Biochem. Sci. *29*, 364–370.
7. Orr, A.W., Helmke, B.P., Blackman, B.R., and Schwartz, M.A. (2006). Mechanisms of mechanotransduction. Dev. Cell *10*, 11–20.
8. Robinson, D.N., and Spudich, J.A. (2004). Mechanics and regulation of cytokinesis. Curr. Opin. Cell Biol. *16*, 182–188.
9. Reichl, E.M., Effler, J.C., and Robinson, D.N. (2005). The stress and strain of cytokinesis. Trends Cell Biol. *15*, 200–206.
10. Robinson, D.N., Cavet, G., Warrick, H.M., and Spudich, J.A. (2002). Quantitation of the distribution and flux of myosin-II during cytokinesis. BMC Cell Biol. *3*, 4.
11. Zhang, W., and Robinson, D.N. (2005). Balance of actively generated contractile and resistive forces controls cytokinesis dynamics. Proc. Natl. Acad. Sci. USA *102*, 7186–7191.
12. Yumura, S. (2001). Myosin II dynamics and cortical flow during contractile ring formation in Dictyostelium cells. J. Cell Biol. *154*, 137–145.
13. Wolpert, L. (1966). The mechanical properties of the membrane of the sea urchin egg during cleavage. Exp. Cell Res. *41*, 385–396.
14. Hiramoto, Y. (1963). Mechanical properties of sea urchin eggs II. Changes in mechanical properties from fertilization to cleavage. Exp. Cell Res. *32*, 76–88.
15. Rappaport, R., and Ebstein, R.P. (1965). Duration of stimulus and latent periods preceding furrow formation in sand dollar eggs. J. Exp. Zool. *158*, 373–382.
16. Hiramoto, Y. (1990). Mechanical properties of the cortex before and during cleavage. Ann. N Y Acad. Sci. *582*, 22–30.
17. Matzke, R., Jacobson, K., and Radmacher, M. (2001). Direct, high-resolution measurement of furrow stiffening during division of adherent cells. Nat. Cell Biol. *3*, 607–610.
18. Wang, Y.L. (2005). The mechanism of cortical ingression during early cytokinesis: Thinking beyond the contractile ring hypothesis. Trends Cell Biol. *15*, 581–588.
19. Shuster, C.B., and Burgess, D.R. (1999). Parameters that specify the timing of cytokinesis. J. Cell Biol. *146*, 981–992.
20. Alsop, G.B., and Zhang, D. (2003). Microtubules continuously dictate distribution of actin filaments and positioning of cell cleavage in grasshopper spermatocytes. J. Cell Sci. *117*, 1591–1602.
21. Brandman, O., Ferrell, J.E., Li, R., and Meyer, T. (2005). Interlinked fast and slow positive feedback loops drive reliable cell decisions. Science *310*, 496–498.
22. Stelling, J., Sauer, U., Szallasi, Z., Doyle, F.J., and Doyle, J. (2004). Robustness of cellular functions. Cell *118*, 675–685.
23. Girard, K.D., Chaney, C., Delannoy, M., Kuo, S.C., and Robinson, D.N. (2004). Dynacortin contributes to cortical viscoelasticity and helps define the shape changes of cytokinesis. EMBO J. *23*, 1536–1546.
24. Girard, K.D., Kuo, S.C., and Robinson, D.N. (2006). Dictyostelium myosin-II mechanochemistry promotes active behavior of the cortex on long time-scales. Proc. Natl. Acad. Sci. USA *103*, 2103–2108.
25. Albertson, R., Riggs, B., and Sullivan, W. (2005). Membrane traffic: A driving force in cytokinesis. Trends Cell Biol. *15*, 92–101.
26. Weber, I., Neujahr, R., Du, A., Köhler, J., Faix, J., and Gerisch, G. (2000). Two-step positioning of a cleavage furrow by cortexillin and myosin II. Curr. Biol. *10*, 501–506.
27. Merkel, R., Simson, R., Simson, D.A., Hohenadl, M., Boulbitch, A., Wallraff, E., and Sackmann, E. (2000). A micromechanic study of cell polarity and plasma membrane cell body coupling in *Dictyostelium*. Biophys. J. *79*, 707–719.
28. Charras, G.T., Yarrow, J.C., Horton, M.A., Mahadevan, L., and Mitchison, T.J. (2005). Non-equilibration of hydrostatic pressure in blebbing cells. Nature *435*, 365–369.
29. Pletjushkina, O.J., Rajfur, Z., Pomorski, P., Oliver, T.N., Vasiliev, J.M., and Jacobson, K. (2001). Induction of cortical oscillations in spreading cells by depolymerization of microtubules. Cell Motil. Cytoskeleton *48*, 235–244.
30. Paluch, E., Piel, M., Prost, J., Bornens, M., and Sykes, C. (2005). Cortical actomyosin breakage triggers shape oscillations in cells and cell fragments. Biophys. J. *89*, 724–733.

Supplemental Data

Mitosis-Specific Mechanosensing and Contractile-Protein Redistribution Control Cell Shape

Janet C. Effler, Yee-Seir Kee, Jason M. Berk, Minhchau N. Tran, Pablo A. Iglesias, and Douglas N. Robinson

Supplemental Experimental Procedures

Strains and Cell Culture

The *Dictyostelium discoideum* strains used were *myoII*(HS1 [S1])::GFP-myoII,G418^R:pBIG; RFP-α-tubulin,Hyg^R:pDRH, *myoII*(HS1)::GFP-myoII,Hyg^R:pDRH; RFP-α-tubulin,Bl^R:pDXA-Bl, *myoII*(HS1)::RFP-α-tubulin,Hyg^R:pDRH, *cortI*(HS1151 [S2])::GFP-cortI,G418^R:pLD1A15SN; RFP-α-tubulin,Hyg^R:pDRH, Ax2::GFP-myoII,G418^R:pBIG; RFP-α-tubulin,Hyg^R:pDRH, and Ax2::GFP-dynacortin,G418^R:pLD1A15SN; RFP-α-tubulin,Hyg^R:pDRH. All cells were grown in HL-5 media with PennStrep, 10–15 μg/ml Hygromycin, and 5–15 μg/ml G418 [S2].

Cell Imaging

Imaging was performed at 22°C ± 0.5°C with a motorized Olympus IX81 microscope with either a 40× NA 1.3 or a 60× NA 1.45 objective, a Xenon lamp, and a Coolsnap HQ CCD camera. MetaMorph imaging software (Molecular Devices) was used to control the microscope and to acquire imaging data. With RFP-α-tubulin, dividing cells were identified by screening for the presence of a mitotic spindle. Upon identification of a dividing cell, the pipette was used to gently dislodge the cell from the glass surface. Negative pressure was applied until the cell exhibited a hemispherical bulge into the glass needle. Unless otherwise indicated, images were collected at 10 s intervals for DIC (10 ms exp), 20 s intervals for GFP-myosin II (100 ms exp), and 40 s intervals for RFP-α-tubulin (200 ms exp).

Construction of Microaspirator

Given that the progression of shape changes of cytokinesis occurs rapidly, the ability to identify dividing cells, position micropipette needles, and apply pressures quickly was crucial. With these design constraints, we built a motorized micropipette aspirator that allowed up to 2 nN/μm^2 pressures (with 10^{-4} nN/μm^2 precision) to be applied within 5 s. A manual linear slide (Bayside Motion Group) was used to position both the adjustable and reference water reservoir tanks at the same height as the pipette tip. The device was calibrated to zero pressure by monitoring the behavior of 1 μm glass beads at the tip of the pipette. When the beads exhibited only Brownian motion, zero pressure was achieved, and the position of the manual linear slide was locked into place. A programmable motorized linear slide (Parker Daedal) was used to lower the adjustable water tank with 10 μm precision. Applied pressures were calculated from the hydrostatic equation, $\Delta P = \rho g h$, where g is the gravitational constant (9.8 m/s^2), h is the differential height between the reference tank and the movable tank, and ρ is the density of water (1000 kg/m^3). Pressures were converted to nN/μm^2.

Microaspiration

Borosilicate capillaries (Sutter outer diameter [O.D.] 1.0 mm, inner diameter [I.D.] 0.75 mm, 10 cm) were pulled to an inner diameter of 4–8 μm (PMP102 Micropipette Puller by MicroData Instruments) and filled with sterile filtered 1× PBS or MES buffer (50 mM MES [pH 6.5], 2 mM $MgCl_2$, 0.2 mM $CaCl_2$). The pipettes were then loaded into a pipette holder (Sutter MI-10010). Micromanipulators (Sutter MP225) allowed submicron positioning of the pipettes. During the loading process, the needle, tubing, and pipette chambers were examined to ensure that air bubbles were not present within the system.

Chambers were prepared by affixing glass cover slides (Fisher 12-545-J 22X60-1) to the bottom of an aluminum anodized chambered plate (70 mm × 32 mm × 2.5 mm) with type M Apiezon grease. Log-phase cells were transferred to imaging chambers and allowed to settle for 15 min. After sufficient time was allowed for the cells to adhere to the glass cover slide, the media was removed, the cells were washed once with 1 ml of MES buffer, and then they were covered with fresh MES buffer. Cells also responded in HL-5 media.

Nocodazole Treatment

To accomplish rapid depolymerization of mitotic microtubules, we grew the cells overnight in HL5 media with 14 mM DMSO. Then, we added 10 μM (final concentration) nocodazole (or an equivalent volume of DMSO) to the cells, which raised the DMSO level to a final concentration of 18 mM, and the microtubules were monitored by following RFP-tubulin. DMSO-treatment did not depolymerize microtubules, and 85% (17 out of 20) of DMSO-treated controls completed cytokinesis normally. In contrast, nocodazole treatment caused the disappearance of mitotic-spindle microtubules in loaded and unloaded cells in 150 ± 13 s (mean ± SEM; n = 26). To ensure that microtubules were depolymerized, we imaged each mitotic cell from top to bottom. Nocodazole treatment caused 92% (11 out of 12) of unloaded cells to fail at cytokinesis. However, interphase microtubules were not obviously disassembled within the timeframe of the experiment. The cells were aspirated after the microtubules disappeared (Figure 3C).

Statistical Analysis of the Responses

For determining the magnitudes of the loaded responses, the images were background subtracted and the mean pixel intensity of the cortex in the pipette (I_p) and of the cortex opposite of the pipette (I_o) were measured with Image J (NIH). For late-stage dividing cells, the opposite cortex was defined as the opposite polar cortex. The ratio of these intensities was calculated. Because the distributions of values were somewhat skewed, we used log-transformed data to calculate all statistics. We used the interphase data to define a response as a $\log(I_p/I_o)$ value greater than 0.14 (corresponding to a real-space I_p/I_o ratio of 1.39), which is the interphase mean plus two standard deviations. With this cutoff for GFP-myosin II, the fraction of responders was determined for each perturbation (Table S1). The GFP-cortexillin-I responses were similarly defined, with GFP-cortexillin-I-expressing interphase cells as the reference.

To quantify the effect of shape asymmetry in unloaded cells early in cytokinesis, we measured asymmetric GFP-myosin distribution before the onset of myosin-II accumulation at the furrow. For analyzing this response, the images were background subtracted and the mean pixel intensity of the cortical response and of the cortex opposite the response were measured with Image J (NIH). The ratio of these intensities was calculated. As defined above, cells with a ratio above 1.39 were classified as responding cells while cells with a ratio below 1.39 were classified as nonresponding cells. The axial ratio (length/width) of each cell at the time point of the response was also calculated.

Supplemental References

S1. Ruppel, K.M., Uyeda, T.Q.P., and Spudich, J.A. (1994). Role of highly conserved lysine 130 of myosin motor domain. In vivo and in vitro characterization of site specifically mutated myosin. J. Biol. Chem. *269*, 18773–18780.

S2. Robinson, D.N., and Spudich, J.A. (2000). Dynacortin, a genetic link between equatorial contractility and global shape control discovered by library complementation of a Dictyostelium discoideum cytokinesis mutant. J. Cell Biol. *150*, 823–838.

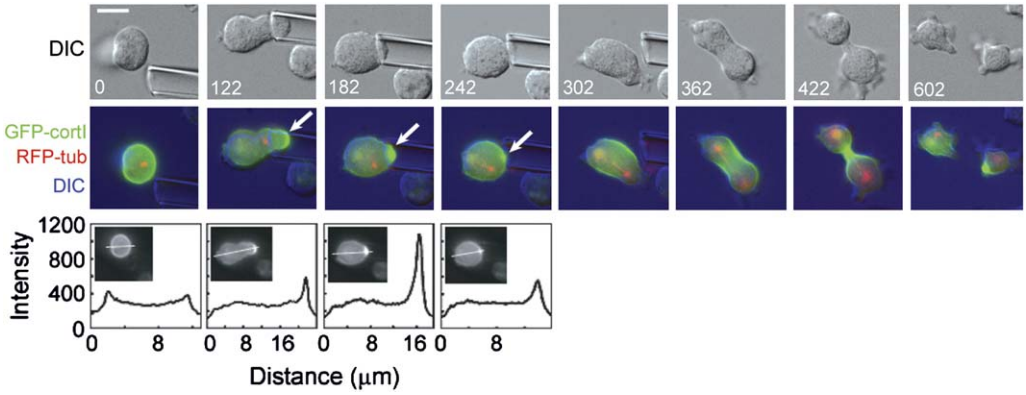

Figure S1. The Contractile Protein Cortexillin I Responds to Applied Load

Before aspiration, GFP-cortexillin I was located uniformly around the cortex (0 s). The cell was aspirated before spindle elongation (0.29 nN/μm^2). As the spindle elongated, GFP-cortexillin I was initially recruited to the pipette (arrows). Though the pressure was constant, the cell escaped the pipette (242 s). Cortexillin-I recruitment to the furrow resumed (362 s), and the cell divided normally (422 s). Line scans show the magnitude of the GFP-cortexillin-I response; insets show the line position. Sixty-seven percent of these cells showed responses (Student's t test: p = 0.043; Table S1). The scale bar represents 10 μm. This image sequence corresponds to Movie S5.

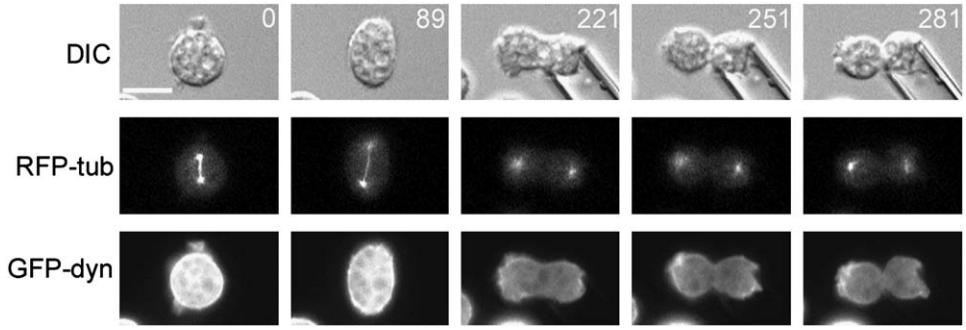

Figure S2. Dynacortin Does Not Respond to Applied Load

The time series shows an aspirated wild-type cell expressing GFP-dynacortin and RFP-α-tubulin (pressure 0.35 nN/μm^2 began at 158 s). None (n = 22) of the cells relocated dynacortin in response to pressures, ranging from 0.15 to 0.35 nN/μm^2. The scale bar represents 10 μm.

Table S1. Frequency of GFP-Myosin-II and GFP-Cortexillin-I Responses

Protein	Cell-Cycle Stage If Load Was Applied	Total Responses	Completed Cytokinesis
GFP-Myosin II			
	Interphase (with Load)	0% (0/17)	NA
	Cytokinesis (no Load)	43% (17/40)	93% (37/40)
	+Noc	NA	8.3% (1/12)
	Cytokinesis (with Load)		
	One pipette	73% (29/40)	95% (38/40)
	Two pipettes	94% (16/17)	NA
	+Noc	57% (8/14)	0% (0/14)
GFP-Cortexillin I			
	Interphase (with Load)	0% (0/5)	NA
	Cytokinesis (no Load)	20% (1/5)	80% (4/5)
	Cytokinesis (with Load)	67% (4/6)	67% (4/6)
Totals (without Noc)			
	Load during interphase	0% (0/22)	NA
	Load in cytokinesis	78% (49/63)[a]	91% (42/46)[b]
	No load in cytokinesis	40% (18/45)[a]	91% (41/45)[c]

NA denotes not applicable.

[a] Response rates between unloaded and loaded cells were significantly different (χ^2 test: $p < 0.001$).

[b] Loaded cells required a longer time than unloaded cells to complete cytokinesis. Also, cells loaded early in cytokinesis typically escaped the pipette before completing cytokinesis, whereas cells loaded late in cytokinesis were able to finish while still under load.

[c] Unloaded cells with symmetric and asymmetric myosin II during early cytokinesis completed cytokinesis within a statistically indistinguishable time frame.

Table S2. Frequency of Unloaded and Loaded *myoII* Cytokinesis Outcomes

	Symmetric Cytokinesis	Asymmetric Cytokinesis[b]	Failed Cytokinesis
Unloaded	41% (16/39)	46% (18/39)	13% (5/39)[c]
Loaded[a]	31% (4/13)	31% (4/13)	38% (5/13)[c]

[a] Pressures ranged from 0.05 to 0.25 nN/μm^2, significantly less than the 0.60 nN/μm^2 able to be applied to wild-type cells.

[b] Unloaded and loaded wild-type cells had 8% and 5%, respectively, asymmetric cell divisions.

[c] The difference between failure rates between loaded and unloaded *myoII* mutants is significant (χ^2 test: $p < 0.05$). Note that the failure rate of unloaded (13%) *myoII* mutants is similar to the failure rate of loaded (9%) and unloaded (7%) wild-type cells (Table S1).